# Multielectron-Ion Coincidence Spectroscopy of Xe in Extreme Ultraviolet Laser Fields: Nonlinear Multiple Ionization via Double Core-Hole States

M. Fushitani[1,2] Y. Sasaki,[1] A. Matsuda,[1,2] H. Fujise,[1,2] Y. Kawabe,[1] K. Hashigaya,[1] S. Owada,[2,3] T. Togashi,[2,3] K. Nakajima,[2,3] M. Yabashi,[2,3] Y. Hikosaka[4,2] and A. Hishikawa[1,5,2,*]

[1]*Department of Chemistry, Graduate School of Science, Nagoya University, Nagoya, Aichi 464-8602, Japan*
[2]*RIKEN, SPring-8 Center, Sayo, Hyogo 679-5148, Japan*
[3]*Japan Synchrotron Radiation Research Institute, Sayo, Hyogo 679-5198, Japan*
[4]*Institute of Liberal Arts and Sciences, University of Toyama, Toyama 930-0194, Japan*
[5]*Research Center for Materials Science, Nagoya University, Nagoya, Aichi 464-8602, Japan*

Ultrafast multiphoton ionization of Xe in strong extreme ultraviolet free-electron laser (FEL) fields (91 eV, 30 fs, $1.6 \times 10^{12}$ W/cm$^2$) has been investigated by multielectron-ion coincidence spectroscopy. The electron spectra recorded in coincidence with Xe$^{4+}$ show characteristic features associated with two-photon absorption to the $4d^{-2}$ double core-hole (DCH) states and subsequent Auger decay. It is found that the pathway via the DCH states, which has eluded clear identification in previous studies, makes a large contribution to the multiple ionization, despite the long FEL pulse duration compared with the lifetime of the $4d$ core-hole states.

Nonlinear responses of matter to extreme ultraviolet (EUV) and x-ray laser fields have attracted increasing attention in recent years, for their importance in various applications of free-electron lasers (FELs), ranging from single particle diffraction imaging to creation of matter in extreme conditions (see, for example, Refs. [1,2]). Isolated atoms and molecules have served as fundamental references to clarify the underlying processes involving ionization and excitation of core electrons in the high frequency laser fields [3–6]. Because of short lifetimes of core-hole states, nonlinear multiphoton absorption proceeds in the presence of Auger (or Coster-Kronig) decay [7–16], which leads to competitions between pathways consisting of different sequences of photoabsorption and Auger decay. Moreover, vacancies created in valence and core orbitals pave additional pathways for photoabsorption, known as "hidden" resonance, which enhances multiple ionization by many orders of magnitude [15–20]. Understanding of nonlinear processes in EUV and x-ray laser fields is still challenging due to the complicated nature.

Photoelectron spectroscopy is powerful in resolving the contributions from different ionization pathways, as intermediate states populated in the multiple ionization can be determined from the kinetic energies of ejected electrons [10,13,18,21–25]. It has been successfully applied to identify characteristic nonlinear pathways via doubly excited states [22] for He and double core-hole (DCH) states for Ne [13,24], CO [26], CO$_2$, N$_2$O, N$_2$ [27], C$_2$H$_2$, and C$_2$H$_6$ [28]. Recently, covariance techniques [24,25] have been introduced to identify correlations between ejected electrons, which enables secure assignments of

ionization pathways. However, in some cases, careful subtraction of strong contributions from single-photon processes is necessary to discriminate nonlinear responses in the spectra [26,27]. Such data analysis could become particularly difficult for heavy element atoms, as the Auger electrons are often distributed in a wide spectral range to mask weak high-order signals.

Here we introduce an alternative approach, coincidence spectroscopy with counterpart ions, which allows direct characterization of electrons emitted in a specific ionization pathway. We revisit multiphoton ionization of Xe in EUV ($\sim$90 eV), which served as a benchmark for elucidating atomic nonlinear responses to EUV FEL fields [7–12]. Because of the large photoabsorption cross sections due to the giant resonance, the ionization is governed by the $4d$ electrons in the initial stages [7–12]. Since the lifetime of the $4d$ single core-hole (SCH) states ($\sim$6 fs) is shorter than a typical FEL pulse duration ($\geq$ 10 fs), the multiple ionization is expected to proceed mainly by alternation of the $4d$ ionization and the subsequent decay [11,12]. Using multielectron-ion coincidence spectroscopy, we present electron spectra for the two-photon multiple ionization to Xe$^{4+}$ in EUV FEL fields ($1.6 \times 10^{12}$ W/cm$^2$). An ionization pathway via the $4d^{-2}$ DCH states, which have eluded identification in previous studies, is clearly observed. It is shown that two-photon ionization to the DCH states makes a major contribution to the multiple ionization to Xe$^{4+}$, despite the long FEL pulse duration.

The experiment was performed at the soft x-ray beam line (BL1) of SACLA [29], which delivers ultrashort EUV pulses at $h\nu = 91$ eV (bandwidth, $\sim$2 eV; pulse duration,
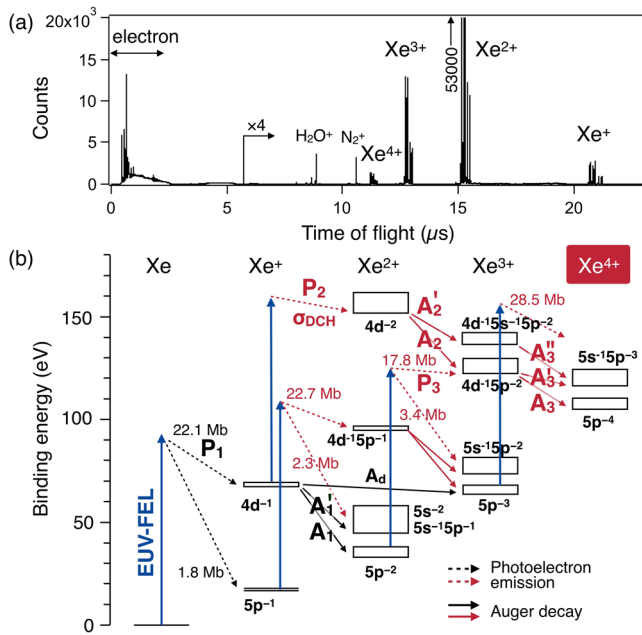
FIG. 1. (a) Time-of-flight spectrum of electrons and ions of Xe in strong EUV-FEL fields (91 eV, $1.6 \times 10^{12}$ W/cm$^2$). The vertical axis represents the number of counts in a time bin (0.5 ns). (b) Energy diagram of electronic states of Xe$^{z+}$ ($z = 0$–4). Arrows represent processes included in numerical simulations. Vertical arrows represent photoabsorption. Photoelectron emission and Auger decay are shown with dotted and solid arrows, respectively. Corresponding photoabsorption cross sections [33–35] are also shown.



FIG. 2. (a) Coincidence photoelectron spectrum recorded with Xe$^{2+}$ in strong EUV-FEL fields (91 eV, $1.6 \times 10^{12}$ W/cm$^2$) (dashed line) and the corresponding covariance spectrum (solid line). The vertical axis represents the number of electron counts in an energy bin (0.18 eV). Sticks represent the energies of the $4d$ photoelectron ($P_1$) and the Auger peaks ($A_1$, $A_1'$) [36,37]. (b) Same as (a) but for Xe$^{4+}$. Sticks represent the major peaks of the Auger processes ($A_2$, $A_2'$, $A_3$, $A_3'$, and $A_3''$) [38] and the $4d$ photoelectrons ($P_2$ and $P_3$) involved in the two-photon ionization to Xe$^{4+}$. The scaled Xe$^{2+}$ covariance spectrum is shown in the bottom ($\alpha = 5.1 \times 10^{-3}$).

30 fs [30]) with a 60 Hz repetition rate. Electron-ion coincidence spectroscopy was carried out by using a magnetic bottle-type electron spectrometer with ion detection capability [31]. Electrons produced from gaseous Xe at the focal spot of EUV pulses were guided by magnetic fields to a microchannel plate (MCP) detector placed at the end of the flight tube. After the arrival of electrons ($\sim 2$ $\mu$s), high voltages were applied to ion-extraction electrodes to detect ions by the same MCP detector. The net gas pressure of Xe was controlled to $\sim 5 \times 10^{-8}$ Pa, to achieve a low average event rate (0.25 events/pulse). To reduce remaining contributions from accidental coincidences, covariance analysis [24,32] was employed.

Figure 1(a) shows the time-of-flight spectrum obtained at a field intensity of $1.6 \times 10^{12}$ W/cm$^2$. The data accumulation time is about 60 h. Electron signals are observed in the time range $\leq 2$ $\mu$s. Ion signals appear later in the spectrum, showing Xe$^{z+}$ ions up to $z = 4$ are produced. The energy diagram in Fig. 1(b) shows that the lower charged ions ($z = 1$–3) can be produced by single photon absorption at the present photon energy (91 eV) [33]. On the other hand, absorption of two EUV photons is needed to form Xe$^{4+}$, which can proceed either by photoionization after the Auger decay of Xe$^+$ $4d^{-1}$ states or by photoionization to $4d^{-2}$ DCH states prior to the Auger decay.
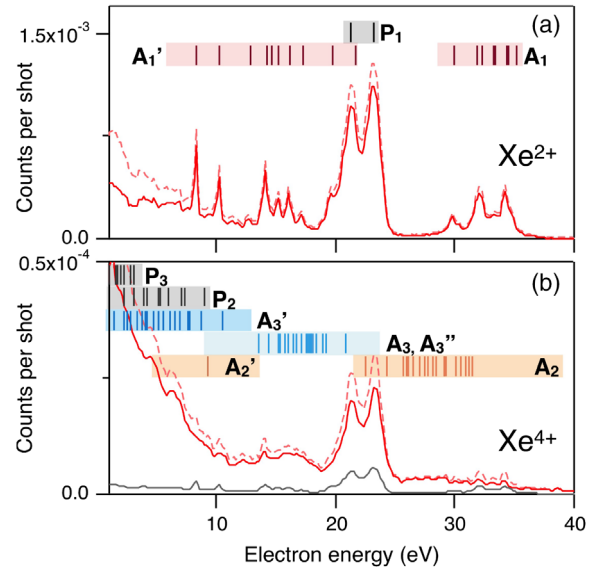
The electron spectrum recorded in coincidence with Xe$^{2+}$ is shown in Fig. 2(a). Prominent peaks are observed at 21.3 and 23.3 eV, which are attributed to photoelectrons by single-photon ionization of the $4d_{3/2}$ and $4d_{5/2}$ inner-shell electrons ($P_1$). Sharp peaks seen in the 8–20 and 28–35 eV region are N$_{4,5}$OO Auger electrons emitted by the decay of the $4d$ core hole ($A_1$ and $A_1'$) to the Xe$^{2+}$ final states [36,37]. These features are clearly seen in the total electron spectrum (not shown), as the Xe$^{2+}$ is the most abundant species in the mass spectra [Fig. 1(a)].

For more quantitative discussion, we carried out covariance analysis [24,32] of the observed spectra. Covariance of two correlated variables is defined as, $\text{Cov}(X, Y) = \langle XY \rangle - \langle X \rangle \langle Y \rangle$, where $\langle X \rangle$ and $\langle Y \rangle$ represent the average of variables $X$ and $Y$ per laser shot, respectively. The first term $\langle XY \rangle$ represents the average number of the coincidence events, while the second term $\langle X \rangle \langle Y \rangle$ corresponds to the accidental coincidence. Figure 2(a) plots the one-dimensional covariance electron spectrum for Xe$^{2+}$, obtained by projection of the two-dimensional covariance map. The features observed in the coincidence spectra are clearly seen in the covariance spectrum. The suppressed low energy components are attributed to secondary electrons from electrode surfaces.

The electron spectrum correlated with Xe$^{4+}$ is shown in Fig. 2(b). In contrast to the Xe$^{2+}$ spectrum, the $A_1$ and $A_1'$

Auger electron peaks are only barely seen, though the $4d$ photoelectron doublet peaks are present in the spectra. Instead, strong distributions appear below 10 eV, together with a structured hump around 16 eV and weak features extending from 25.5 to 38 eV. This indicates that the sequential SCH (seq-SCH) pathway associated with the photoionization after the $A_1$ and $A_1'$ Auger decay has only a minor contribution.

The decay pathways of the Xe $4d^{-2}$ DCH states have been investigated by soft x-ray single-photon absorption study [38,39]. As shown in Fig. 1(b), the DCH states of $Xe^{2+}$ mainly decay to the $Xe^{3+}$ $(4d^{-1}5p^{-2})$ states by emitting Auger electrons $(A_2)$ in the 25.5–38 eV energy region. The $Xe^{3+}$ states decay further to the $5s^{-1}5p^{-3}$ states or to the $5p^{-4}$ states of $Xe^{4+}$, with Auger electrons of 0–12 eV $(A_3')$ and 10–24 eV $(A_3)$, respectively. The features observed in the electron spectrum of $Xe^{4+}$ appear in the same energy region of these Auger electrons, though the individual peaks are not fully resolved due to the limited resolution of the spectrometer $(E/\Delta E \sim 40)$. Photoelectron energies expected for the second photon absorption from the $4d^{-1}$ SCH states $(P_2)$ are calculated from the energies of the two spin-orbit levels of $Xe^+$ $4d^{-1}$ state and the nine states in the $Xe^{2+}$ $4d^{-2}$ configuration [40]. The obtained results are plotted in Fig. 2(b), showing that the photo-electrons fall in the strong broad feature in the energy region $< 9$ eV.

The proposed multiple ionization pathways can be verified by the correlation between the ejected electrons. Figure 3 shows the electron-electron correlation maps for $Xe^{2+}$ and $Xe^{4+}$, obtained as the triple covariance of two electrons and one ion, $\text{Cov}(X, Y, Z) = \langle (X - \langle X \rangle)(Y - \langle Y \rangle)(Z - \langle Z \rangle) \rangle = \text{Cov}(XY, Z) - \langle X \rangle \text{Cov}(Y, Z) - \langle Y \rangle \text{Cov}(X, Z)$ [32]. For $Xe^{2+}$, clear correlations between the spin-orbit states populated by the $4d$ photoionization $(P_1)$ and the Auger electrons $(A_1$ and $A_1')$ are observed [41,42].

As for $Xe^{4+}$, the correlation is barely visible in Fig. 3(b). Instead, the photoelectron peaks show clear correlations with the low energy component containing the second photoelectron peaks $(P_2)$, as expected for the ionization to the DCH states. Correlations between the photoelectron $(P_1$ or $P_2)$ and the Auger electron $(A_2, A_3$ or $A_3')$ are also clearly seen in the map, together with those between the $A_2$ Auger electron and the $A_3$ or $A_3'$ Auger electron.

It is worth noting that clear diagonal ridges are visible in the map at a total energy of $\sim 34$ eV. The ridges can be attributed to the energy sharing between the photoelectron $(P_2)$ and the Auger electron $(A_2)$ emitted via the inter-mediate $4d^{-2}$ DCH states. For the lowest states in the corresponding configurations, $E(4d^{-1}\,^2D_{5/2}) = 67.5$ eV and $E(4d^{-1}5p^{-2}\,^4F_{9/2}) = 122.4$ eV [38], the surplus energy shared by the two electrons is estimated to be $E(4d^{-1}) + h\nu - E(4d^{-1}5p^{-2}) = 36$ eV. The obtained energy is in good agreement with the observed total energy, confirming the multiple ionization pathway via the $4d^{-2}$ DCH states.
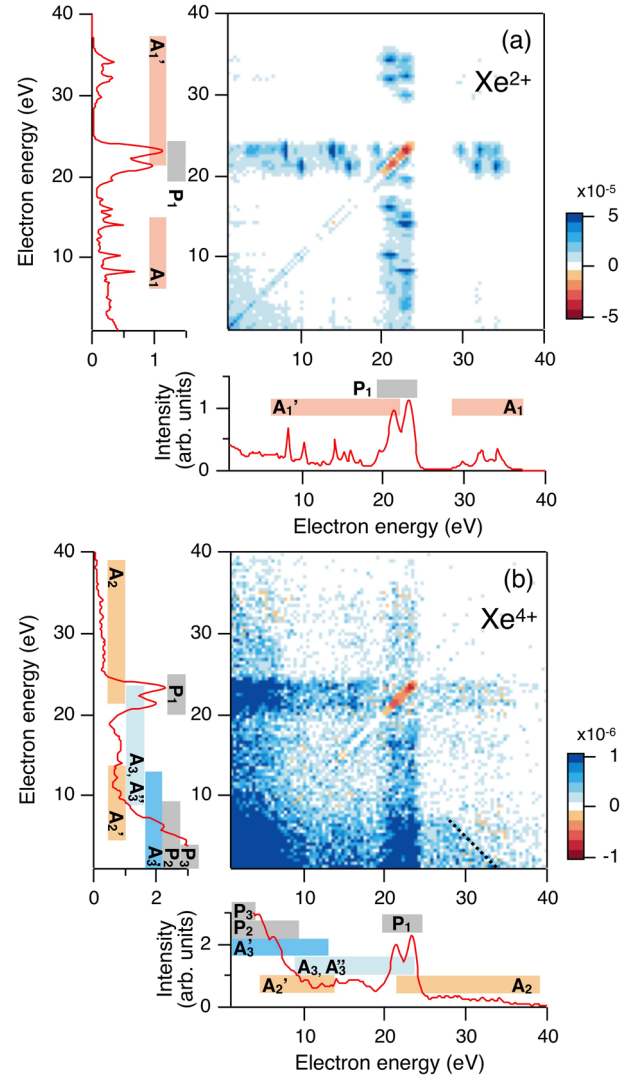


FIG. 3. Electron-electron correlation map for (a) $Xe^{2+}$ and (b) $Xe^{4+}$ obtained by the triple covariance analysis. The color scale represents the counts per shot. Corresponding photoelectron spectra are shown along the horizontal and vertical axes. The position of the diagonal ridges observed at a total energy of 34 eV is also shown in the bottom right half of the map (dotted line).

In the correlation map, diagonal-line distributions expected for the double Auger decay to $Xe^{3+}$ [43] are essentially absent (see Supplemental Material [44]). This shows that the sequential ionization via $Xe^{3+}$ has a negligible contribution to the two-photon ionization to $Xe^{4+}$. Therefore the competing process (seq-SCH) is likely to proceed through photoionization from $5p^{-2}$ to $4d^{-1}5p^{-2}$ because of the large cross section, which is followed by the $A_3$ and $A_3'$ decay [see Fig. 1(b)]. The corresponding photoelectron $(P_3)$ is expected to appear with $E \leq 5$ eV, which falls in the low energy feature in Figs. 2 and 3.

The branching fraction of these pathways is estimated from the relative yields of the corresponding Auger electrons, $A_1$, $A_1'$ and $A_2$, in Fig. 2(b). Details are given

in Supplemental Material [44]. Briefly, the $Xe^{2+}$ spectrum is scaled by least squares fitting to selected $A_1$ Auger peaks (at 32 and 34 eV) in the $Xe^{4+}$ spectrum. Two cases are considered, with and without background contributions, which provides the lower and upper boundary of the scaling factor $\alpha = 5.1(7) \times 10^{-3}$ and $9.1(7) \times 10^{-3}$. The bottom trace in Fig. 2(b) is the $Xe^{2+}$ spectrum obtained with the former scaling factor. The relative yield $S(A_1')$ and $S(A_1)$ is then obtained by integration of the scaled $Xe^{2+}$ spectrum in the corresponding energy ranges to derive the total yields for the seq-SCH pathway, $S_{\mathrm{seqSCH}}$. The net yield $S(A_2)$ for $A_2$ is obtained from the $Xe^{4+}$ spectrum after subtraction of the scaled $Xe^{2+}$ spectrum. The decay pathway via $Xe^{3+}$ $4d^{-1}5s^{-1}5p^{-1}$ states $(A_2')$ is also taken into account to derive the total yield of the DCH pathway, $S_{\mathrm{DCH}}$. The branching fractions for the DCH pathway are then calculated to be $\Phi = S_{\mathrm{DCH}}/(S_{\mathrm{DCH}} + S_{\mathrm{seqSCH}}) = 0.60(4)$ and $0.40(3)$ for the two scaling factors, respectively, which shows that the contribution from the DCH pathway is comparable with or even larger than the seq-SCH pathway.

Since the photoabsorption to the DCH states competes with the ultrafast Auger decay of the $4d^{-1}$ SCH states ($\sim 6$ fs [45]), the long duration of the FEL pulse (30 fs) does not favor the DCH pathway [11,12]. To understand the two-photon ionization to $Xe^{4+}$, we carried out numerical simulations solving coupled rate equations. The included processes are shown in Fig. 1(b) with the relevant photoabsorption cross sections [33–35]. The lifetime of the $4d$ core-hole states is set to 6 fs irrespective of the charged states. Variation of the FEL field intensity around the focus (volume effect) is taken into account [21]. The unknown photoabsoption cross section $\sigma_{\mathrm{DCH}}$ from $Xe^{+}(4d^{-1})$ to $Xe^{2+}$ $(4d^{-2})$ is treated as an adjustable parameter. Figure 4(a) shows calculated branching fractions $\Phi$, plotted as a function of $\sigma_{\mathrm{DCH}}$. The observed upper boundary $\Phi = 0.60(4)$ corresponds to $\sigma_{\mathrm{DCH}} = 64^{+14}_{-11}$ Mb, while $\sigma_{\mathrm{DCH}} = 27^{+4}_{-4}$ Mb is obtained at the lower boundary $\Phi = 0.40(3)$ [44]. Experimental ion yields in Fig. 4(b) are well reproduced with $\sigma_{\mathrm{DCH}}$ in the range between these values.

The obtained results suggest that $\sigma_{\mathrm{DCH}}$ is considerably larger than the normal $4d$ cross sections ($\sim 20$ Mb). The enhancement could be attributed to the resonance excitation from the $4d^{-1}$ to $4p^{-1}$ states in $Xe^{+}$ [40]. Because of strong interactions with the $4d^{-2}mf$ states and $4d^{-2}\epsilon f$ continuum [46], the $4p^{-1}$ states spread over 30 eV near the $4d^{-2}$ ionization threshold ($\sim 160$ eV). The interactions transfer about 90% of the $4p^{-1}_{1/2}$ intensity and about 50% of the $4p^{-1}_{3/2}$ intensity into the $4d^{-2}$ continuum. The broad spectrum, associated with the breakdown of the quasiparticle picture for the $4p^{-1}$ core hole, fully covers the spectral bandwidth of the FEL ($\sim 2$ eV). Thus, the core-to-core resonance $4d^{-1} \to 4p^{-1}$ can efficiently occur and enhance the ionization to the DCH states by "virtual" super Coster-Kronig transition [39,46].



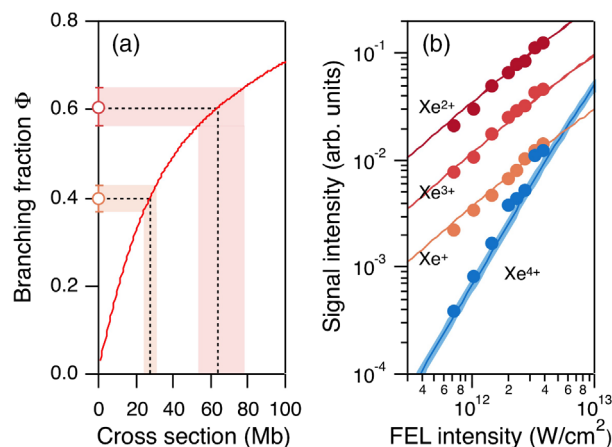FIG. 4. (a) Branching fraction $\Phi$ for the DCH pathway plotted against the photoabsorption cross section to the DCH states, $\sigma_{\mathrm{DCH}}$, obtained by numerical simulations solving coupled rate equation (solid line). The upper and lower bound values $\Phi = 0.60(4)$ and $0.40(3)$ at $1.6 \times 10^{12}$ W/cm² is shown with the estimated uncertainties, which corresponds to $\sigma_{\mathrm{DCH}} = 64$ and 27 Mb, respectively. (b) FEL intensity dependence of the Xe ion yields (circle). The results of the simulation are also shown (solid line). The upper and lower bounds of the shaded area for $Xe^{4+}$ correspond to those of $\sigma_{\mathrm{DCH}}$, respectively.

In summary, we employed multielectron-ion coincidence spectroscopy to study two-photon ionization pathways of Xe in EUV FEL fields. It is shown that the $4d^{-2}$ DCH pathway, which has eluded clear identification, has an unexpectedly large contribution in the two-photon ionization to $Xe^{4+}$. The Auger decay from DCH states is known to sensitively reflect a local chemical environment around atomic sites within a molecule [47,48]. The present technique, powerful in elucidating nonlinear processes of atoms and molecules in strong EUV and x-ray FEL fields, would provide an indispensable approach to further explore this unique property for chemical analysis.

*hishi@chem.nagoya-u.ac.jp
[1] C. Bostedt, S. Boutet, D. M. Fritz, Z. Huang, H. J. Lee, H. T. Lemke, A. Robert, W. F. Schlotter, J. J. Turner, and G. J. Williams, Rev. Mod. Phys. **88**, 015007 (2016).

[2] E. A. Seddon, J. A. Clarke, D. J. Dunning, C. Masciovecchio, C. J. Milne, F. Parmigiani, D. Rugg, J. C. H. Spence, N. R. Thompson, K. Ueda, S. M. Vinko, J. S. Wark, and W. Wurth, Rep. Prog. Phys. **80,** 115901 (2017).

[3] M. Yabashi, H. Tanaka, T. Tanaka, H. Tomizawa, T. Togashi, M. Nagasono, T. Ishikawa, J. R. Harries, Y. Hikosaka, A. Hishikawa, K. Nagaya, N. Saito, E. Shigemasa, K. Yamanouchi, and K. Ueda, J. Phys. B **46,** 164001 (2013).

[4] J. Feldhaus, M. Krikunova, M. Meyer, Th. Möller, R. Moshammer, A. Rudenko, Th. Tschentscher, and J. Ullrich, J. Phys. B **46,** 164002 (2013).

[5] C. Bostedt et al., J. Phys. B **46,** 164003 (2013).

[6] L. Young et al., J. Phys. B **51,** 032003 (2018).

[7] A. A. Sorokin, S. V. Bobashev, T. Feigl, K. Tiedtke, H. Wabnitz, and M. Richter, Phys. Rev. Lett. **99,** 213002 (2007).

[8] M. Richter, M. Y. Amusia, S. V. Bobashev, T. Feigl, P. N. Juranić, M. Martins, A. A. Sorokin, and K. Tiedtke, Phys. Rev. Lett. **102,** 163002 (2009).

[9] M. Krikunova, T. Maltezopoulos, A. Azima, M. Schlie, U. Frühling, H. Redlin, R. Kalms, S. Cunovic, N. M. Kabachnik, M. Wieland, and M. Drescher, New J. Phys. **11,** 123019 (2009).

[10] V. Richardson, J. T. Costello, D. Cubaynes, S. Düsterer, J. Feldhaus, H. W. van der Hart, P. Juranić, W. B. Li, M. Meyer, M. Richter, A. A. Sorokin, and K. Tiedtke, Phys. Rev. Lett. **105,** 013001 (2010).

[11] P. Lambropoulos, K. G. Papamihail, and P. Decleva, J. Phys. B **44,** 175402 (2011).

[12] S. Fritzsche, A. N. Grum-Grzhimailo, E. V. Gryzlova, and N. M. Kabachnik, J. Phys. B **44,** 175602 (2011).

[13] L. Young et al., Nature (London) **466,** 56 (2010).

[14] H. Fukuzawa et al., Phys. Rev. Lett. **110,** 173005 (2013).

[15] B. Rudek et al., Nat. Photonics **6,** 858 (2012).

[16] B. Rudek et al., Phys. Rev. A **87,** 023413 (2013).

[17] G. Doumy et al., Phys. Rev. Lett. **106,** 083002 (2011).

[18] E. P. Kanter et al., Phys. Rev. Lett. **107,** 233001 (2011).

[19] P. J. Ho, C. Bostedt, S. Schorb, and L. Young, Phys. Rev. Lett. **113,** 253001 (2014).

[20] P. J. Ho, E. P. Kanter, and L. Young, Phys. Rev. A **92,** 063430 (2015).

[21] Y. Hikosaka, M. Fushitani, A. Matsuda, C. M. Tseng, A. Hishikawa, E. Shigemasa, M. Nagasono, K. Tono, T. Togashi, H. Ohashi, H. Kimura, Y. Senba, M. Yabashi, and T. Ishikawa, Phys. Rev. Lett. **105,** 133001 (2010).

[22] A. Hishikawa, M. Fushitani, Y. Hikosaka, A. Matsuda, C.-N. Liu, T. Morishita, E. Shigemasa, M. Nagasono, K. Tono, T. Togashi, H. Ohashi, H. Kimura, Y. Senba, M. Yabashi, and T. Ishikawa, Phys. Rev. Lett. **107,** 243003 (2011).

[23] M. Fushitani, Y. Hikosaka, A. Matsuda, T. Endo, E. Shigemasa, M. Nagasono, T. Sato, T. Togashi, M. Yabashi, T. Ishikawa, and A. Hishikawa, Phys. Rev. A **88,** 063422 (2013).

[24] L. J. Frasinski et al., Phys. Rev. Lett. **111,** 073002 (2013).

[25] V. Zhaunerchyk et al., J. Phys. B **48,** 244003 (2015).

[26] N. Berrah, L. Fang, B. Murphy, T. Osipov, K. Ueda, E. Kukk, R. Feifel, P. van der Meulen, P. Salen, H. T. Schmidt, R. D. Thomas, M. Larsson, R. Richter, K. C. Prince, J. D. Bozek, C. Bostedt, S.-i. Wada, M. N. Piancastelli, M. Tashiro, and M. Ehara, Proc. Natl. Acad. Sci. U.S.A. **108,** 16912 (2011).

[27] P. Salén, P. van der Meulen, H. T. Schmidt, R. D. Thomas, M. Larsson, R. Feifel, M. N. Piancastelli, L. Fang, B. Murphy, T. Osipov, N. Berrah, E. Kukk, K. Ueda, J. D. Bozek, C. Bostedt, S. Wada, R. Richter, V. Feyer, and K. C. Prince, Phys. Rev. Lett. **108,** 153003 (2012).

[28] M. Mucke et al., New J. Phys. **17,** 073002 (2015).

[29] S. Owada, K. Togawa, T. Inagaki, T. Hara, T. Tanaka, Y. Joti, T. Koyama, K. Nakajima, H. Ohashi, Y. Senba, T. Togashi, K. Tono, M. Yamaga, H. Yumoto, M. Yabashi, H. Tanaka, and T. Ishikawa, J. Synchrotron Radiat. **25,** 282 (2018).

[30] S. Owada, M. Fushitani, A. Matsuda, H. Fujise, Y. Sasaki, Y. Hikosaka, A. Hishikawa, and M. Yabashi, J. Synchrotron Radiat. (to be published).

[31] A. Matsuda, M. Fushitani, C.-M. Tseng, Y. Hikosaka, J. H. Eland, and A. Hishikawa, Rev. Sci. Instrum. **82,** 103105 (2011).

[32] V. Zhaunerchyk, L. J. Frasinski, J. H. D. Eland, and R. Feifel, Phys. Rev. A **89,** 053418 (2014).

[33] U. Becker, D. Szostak, H. G. Kerkhoff, M. Kupsch, B. Langer, R. Wehlitz, A. Yagishita, and T. Hayaishi, Phys. Rev. A **39,** 3902 (1989).

[34] P. Andersen, T. Andersen, F. Folkmann, V. K. Ivanov, H. Kjeldsen, and J. B. West, J. Phys. B **34,** 2009 (2001).

[35] J. M. Bizau, C. Blancard, D. Cubaynes, F. Folkmann, J. P. Champeaux, J. L. Lemaire, and F. J. Wuilleumier, Phys. Rev. A **73,** 022718 (2006).

[36] T. X. Carroll, J. D. Bozek, E. Kukk, V. Myrseth, L. J. Saethre, T. D. Thomas, and K. Wiesner, J. Electron Spectrosc. Relat. Phenom. **125,** 127 (2002).

[37] A. Kivimäki, L. Pfeiffer, H. Aksela, E. Nõmmiste, and S. Aksela, J. Electron Spectrosc. Relat. Phenom. **101–103,** 43 (1999).

[38] V. Jonauskas, L. Partanen, S. Kučas, R. Karazija, M. Huttula, S. Aksela, and H. Aksela, J. Phys. B **36,** 4403 (2003).

[39] Y. Hikosaka, P. Lablanquie, F. Penent, T. Kaneyasu, E. Shigemasa, J. H. D. Eland, T. Aoto, and K. Ito, Phys. Rev. Lett. **98,** 183002 (2007).

[40] S. Svensson, N. Mårtensson, E. Basilier, P. Å. Malmquist, U. Gelius, and K. Siegbahn, Phys. Scr. **14,** 141 (1976).

[41] J. Viefhaus, M. Braune, S. Korica, A. Reinköster, D. Rolles, and U. Becker, J. Phys. B **38,** 3885 (2005).

[42] M. Fushitani, A. Matsuda, and A. Hishikawa, J. Electron Spectrosc. Relat. Phenom. **184,** 561 (2012).

[43] F. Penent, J. Palaudoux, P. Lablanquie, L. Andric, R. Feifel, and J. H. D. Eland, Phys. Rev. Lett. **95,** 083002 (2005).

[44] See Supplemental Material at http://link.aps.org/supplemental/10.1103/PhysRevLett.124.193201 for details.

[45] M. Uiberacker, Th. Uphues, M. Schultze, A. J. Verhoef, V. Yakovlev, M. F. Kling, J. Rauschenberger, N. M. Kabachnik, H. Schröder, M. Lezius, K. L. Kompa, H. G. Muller, M. J. J. Vrakking, S. Hendel, U. Kleineberg, U. Heinzmann, M. Drescher, and F. Krausz, Nature (London) **446,** 627 (2007).

[46] G. Wendin and M. Ohno, Phys. Scr. **14,** 148 (1976).

[47] L. S. Cederbaum, F. Tarantelli, A. Sgamellotti, and J. Schirmer, J. Chem. Phys. **85,** 6513 (1986).

[48] M. Tashiro, M. Ehara, H. Fukuzawa, K. Ueda, C. Buth, N. V. Kryzhevoi, and L. S. Cederbaum, J. Chem. Phys. **132,** 184302 (2010).